Materialia 21 (2022) 101297

Contents lists available at ScienceDirect

Materialia

journal homepage: www.elsevier.com/locate/mtla

Development and testing of a $Ni_{50.5}Ti_{27.2}Hf_{22.3}$ high temperature shape memory alloy

G.S. Bigelow[a,*], A. Garg[a,b], O. Benafan[a], R.D. Noebe[a], S.A. Padula II[a], D.J. Gaydosh[a,c]

[a] Materials and Structures Division, NASA Glenn Research Center, 21000 Brookpark Rd, Cleveland, OH 44135, USA
[b] University of Toledo, 2801 W. Bancroft, Toledo, OH 43606, USA
[c] Ohio Aerospace Institute, 22800 Cedar Point Road, Cleveland, OH 44142, USA

ARTICLE INFO

Keywords:
Shape memory alloys
Martensitic phase transformation
Precipitation
NiTiHf
H-phase
Transformation strain

ABSTRACT

A NiTiHf alloy with a composition of $Ni_{50.5}Ti_{27.2}Hf_{22.3}$ (at%) was heat treated at various temperatures between 400 and 550 °C at times ranging from 1 to 51 h to determine the effect of aging on its thermomechanical properties. Uniaxial constant-force thermal cycling was performed to determine the transformation temperature, transformation strain, and dimensional stability. Through appropriate heat treatment, the initial austenite finish temperature of 126 °C could be increased to over 200 °C, and the dimensional stability improved to near 0% residual strain through precipitation strengthening, without a significant loss in transformation strain.

1. Introduction

Ni-rich NiTiHf high temperature shape memory alloys (HTSMAs) have emerged as a potential alloy for actuation applications, where both high temperature and superior shape memory properties can be achieved. Ni-rich NiTiHf alloys have been shown to exhibit good dimensional and thermal stability, reasonable transformation strains, and exceptional two-way shape memory response, all of which can occur at moderate transformation temperatures [1–15]. This combination of outstanding mechanical and functional behavior has been attributed to the effect of Hf addition on solid solution strengthening and on precipitation strengthening via a fine, nanometer size precipitate phase known as H-phase [16,17] that strengthens the matrix and resists plastic deformation without hindering twin motion [5].

The most intently studied composition has been the $Ni_{50.3}Ti_{29.7}Hf_{20}$ at.% alloy [1–4,6–10,21]. When aged for three hours at 550 °C, the material exhibits transformation temperatures centered around 150 °C, depending on exact composition, while displaying most of the benefits mentioned above. Therefore, the baseline polycrystalline $Ni_{50.3}Ti_{29.7}Hf_{20}$ alloy provides a significant improvement over the highest available transformation temperature for binary NiTi alloys and serves a critical niche in automotive and aeronautic applications with high temperature requirements. Furthermore, by following similar design strategies (slightly Ni-rich compositions) but with increased Hf contents >24%, it is possible to develop alloys with transformation temperatures greater than 200 °C [15] and recently, greater than 400 °C in a single crystal [13] and polycrystalline material [20]. This allows the NiTiHf alloy to be used in many more high temperature applications where NiTi cannot be used.

In surveying existing literature, there exists very limited research on NiTiHf with compositions above 20 at.% Hf. Additionally, from those reported, only a very small fraction report on the thermomechanical behavior of these alloys. NiTiHf polycrystalline alloys with higher Hf and higher Ni content can offer elevated activation temperature and at the same time can provide improved actuation performance demonstrated via work output and dimensional stability. Therefore, the purpose of this research is to examine a Ni-rich 22.3Hf alloy and study the extent of temperature modification possible when aging at temperatures between 400 and 550 °C for various times. The effects of these heat treatments on the microstructure, and the resulting thermomechanical properties are reported.

2. Material and methods

A Ni-rich HTSMA with a target composition of $Ni_{50.5}Ti_{27.2}Hf_{22.3}$ (at.%) (NASA alloy Ext. 195) was produced via vacuum induction melting of high purity elemental materials (99.98% Ni, 99.95% Ti, and 99.9% Hf (wt%)) under a protective argon atmosphere in a graphite crucible. The molten alloy was cast into a copper mold to form an ingot with dimensions of 25.4 mm in diameter by 102 mm long. Vacuum homogenization of the ingot at 1050 °C for 72 h was followed by extrusion at 900 °C at a 7:1 area reduction ratio. For mechanical testing, cylindrical dog-bone shaped samples with threaded button ends and a 5 mm diameter by 17.8 mm long gage section were machined on a CNC lathe from the extruded material. The machined samples were double

* Corresponding author.
E-mail address: glen.s.bigelow@nasa.gov (G.S. Bigelow).

https://doi.org/10.1016/j.mtla.2021.101297
Received 16 November 2021; Accepted 5 December 2021
Available online 6 December 2021
2589-1529/Published by Elsevier B.V. on behalf of Acta Materialia Inc.

wrapped in Ta foil and aged at temperatures between 400 and 550 °C under flowing argon for varying times (1–51 h) followed by air cooling. These aging conditions are listed in Table 1.

Thermomechanical characterization in tension was performed on an MTS 810 servo-hydraulic frame via uniaxial constant-force thermal cycling (UCFTC) between 30 and 350 °C at constant engineering stress levels of 0 MPa (no-load), 50 MPa, and 100 MPa to 500 MPa in increments of 100 MPa. Heating was performed using an Ameritherm NovaStar induction heater coupled to a Eurotherm controller. Strain was measured via an MTS 632.51B-04 high temperature extensometer. At each stress level, the sample was loaded to the desired stress at 30 °C in the martensite state and then thermally cycled twice. The stress was then incremented to the next load level and the process repeated. Data from the second thermal cycle at each stress level was used to measure residual strain (a measure of dimensional stability), transformation temperatures, and transformation strain.

Compositional analysis of the alloy with target composition $Ni_{50.5}Ti_{27.2}Hf_{22.3}$ was performed using Inductively Coupled Plasma-Atomic Emission Spectroscopy (ICP-AES). The measured composition of the alloy was $Ni_{50.89}Ti_{26.85}Hf_{22.26}$(± 2% of the measured composition) which is slightly more Ni-rich than the target composition of 50.5 at.% Ni. Microstructures of the as-extruded and the aged samples were analyzed in a Hitachi S4700 SEM, and a FEI Talos F200S TEM operating at 200 kV.

3. Results and discussion

In the SEM, the general microstructure of the as-extruded and the aged samples were analogous showing a martensite matrix containing a dispersion of micron-size particles (Fig. 1a). The majority of these particles were identified as HfC (Fig. 1b), although occasionally a HfO_2 particle was also observed. Contamination of C from the graphite crucible used for melting the alloy is likely the cause of HfC formation in the alloy. In TEM, the as-extruded material showed a B19' twinned martensite matrix and submicron-size HfC particles, but no other fine precipitates were observed (Fig. 1c). Microstructure of the 550 °C/3h aged sample, shown in Fig. 1d, was very similar to that of the as-extruded sample except that it also contained a high density of very fine precipitates (size ~15 nm) throughout the matrix (Fig. 1e). These precipitates were identified as H-phase precipitates and a typical diffraction pattern taken from the alloy is shown in Fig.1f. For a detailed characterization of this phase in a Ni-rich Hf_{20} alloy, the reader is referred to the work by Yang et al. [16]. The H-phase has a face-centered orthorhombic structure with lattice parameters a= 1.264 nm, b = 0.882 nm, c = 2.608 nm, and space group of F 2/d 2/d 2/d. It nucleates coherently in the NiTiHf matrix, provides considerable precipitate strengthening to the alloy, and being Ni-rich, depletes the matrix of Ni, thus increasing the transformation temperature of the alloy at the same time.

Fig. 2a depicts the transformation behavior of the 550°C/3h aged condition showing increasing transformation strain and temperatures with increasing applied stress. For all stress conditions, actuation properties were measured using linear regression methods as as outlined in the ASTM standard E3097 [18]. In the as-extruded condition, the no-load (UCFTC) M_F, M_S, A_S, and A_F are 77, 90, 114, and 126 °C, respectively. For comparison between the aging conditions, Fig. 2b shows the as-extruded and heat treated samples during thermal cycling at the 300 MPa constant stress level. In the 400 °C/51 h aged sample, the austenite transformation temperatures dropped by 10 °C compared to the as-extruded condition, and a narrowed hysteresis was observed. With higher temperature aging, there is a corresponding increase in all transformation temperatures, although for the aging conditions studied here, the aging treatments at 500 and 550 °C had a greater effect than those at 400 and 450 °C, despite the shorter aging times. When aged at 550 °C, there is an initially rapid precipitation of the H-phase, the kinetics of which are accelerated by higher temperature, high Hf content, and initial oversaturation of nickel [17,19] as evidenced by increased

Table 1
Transformation Temperatures (°C), Hysteresis, and Thermal Transformation Span for Aged $Ni_{50.5}Ti_{27.2}Hf_{22.3}$ at 0 MPa and 300 MPa from Uniaxial Constant-Force Thermal Cycling as a Function of the Heat Treat Condition.

	No Load						300MPa					
Condition	M_F	M_S	A_S	A_F	Hysteresis(A_F-M_S)	Thermal Transformation Span (A_F-M_F)	M_F	M_S	A_S	A_F	Hysteresis(A_F-M_S)	Thermal Transformation Span (A_F-M_F)
As-extruded	77	90	114	126	36	49	93	112	135	150	38	57
400 °C/51 h	77	87	105	116	29	39	102	123	129	140	17	38
450 °C/10 h	98	107	126	133	26	35	125	143	149	159	16	34
500 °C/3 h	131	138	157	161	23	30	148	171	172	188	17	40
550 °C/1 h	138	150	161	179	29	41	156	179	181	197	18	41
550 °C/3 h	172	178	206	209	31	37	188	210	221	235	25	47
550 °C/10 h	175	180	208	213	33	38	188	212	223	237	25	49
20Hf 550 °C/3 h	128	137	155	166	29	38	150	165	177	187	23	37

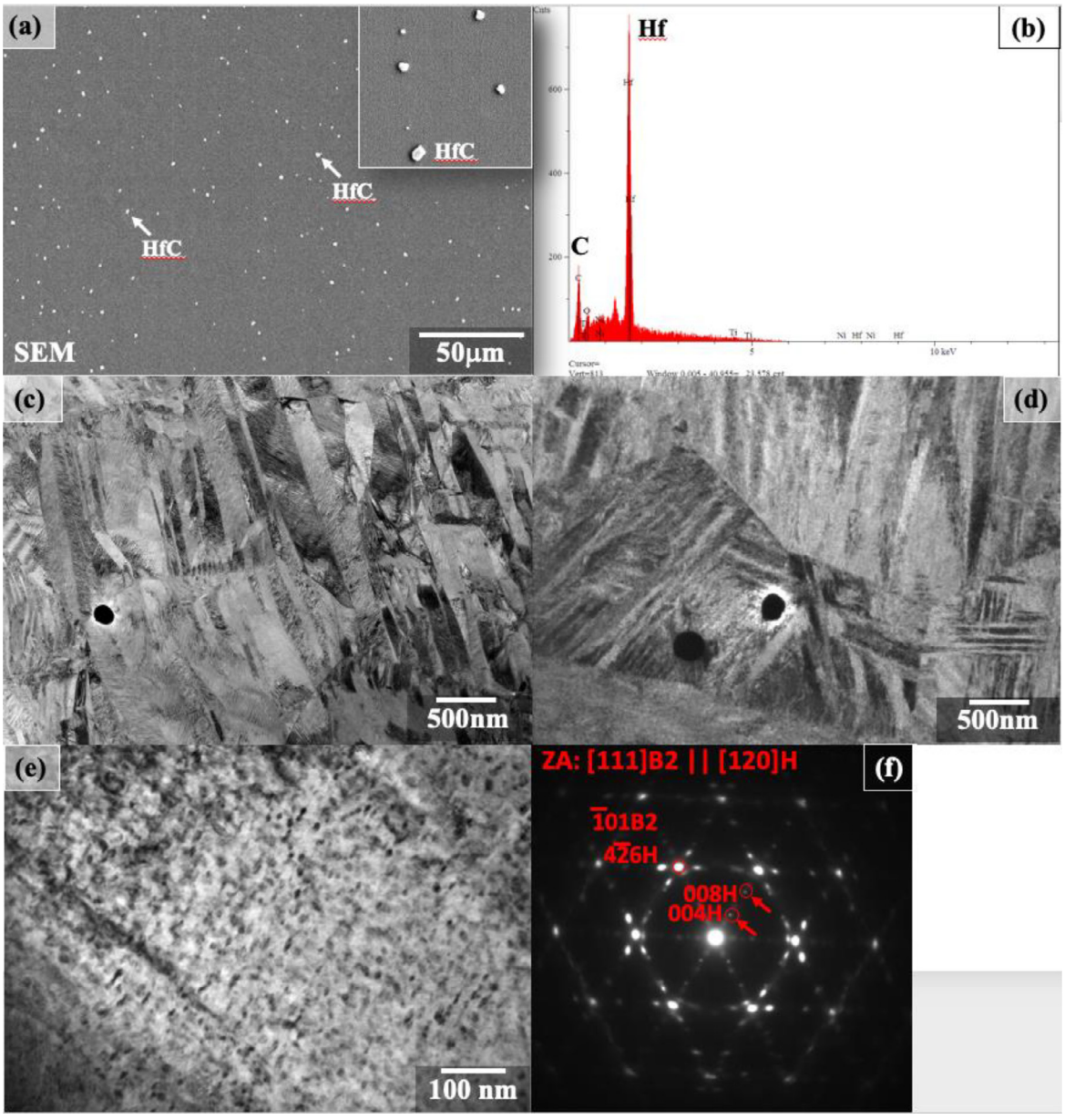

Fig. 1. (a) SEM view of the general microstructure, (b) EDS of the white particles in (a), TEM microstructures of the (c) as-extruded and (d) the aged alloy, (e) fine precipitates in the aged alloy, (f) selected areas diffraction pattern of the aged alloy shown in (d,e) confirming the presence of H-phase.

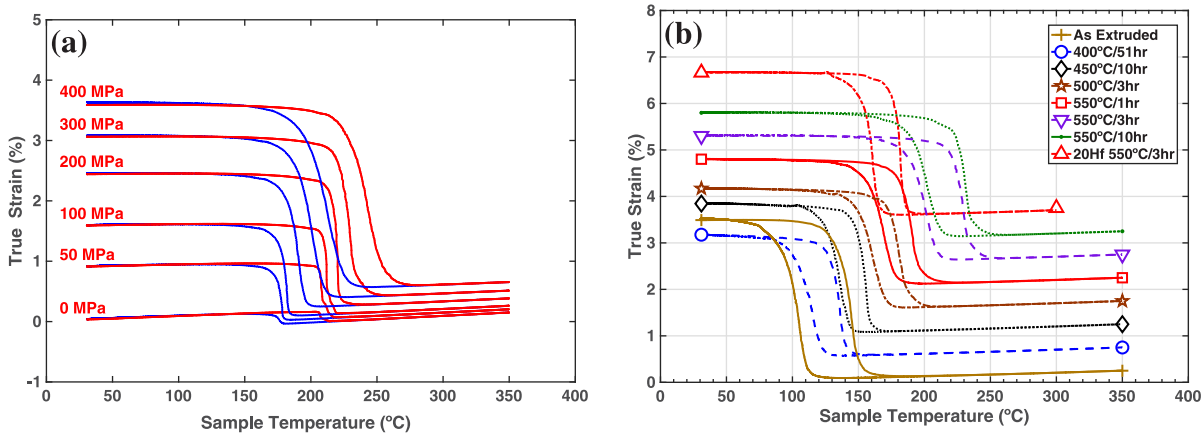

Fig. 2. (a) Constant force shape memory behavior of 550 °C/3h $Ni_{50.5}Ti_{27.2}$ $Hf_{22.3}$ in tension, (b) comparison of transformation behavior under 300MPa tensile stress for all aging conditions.

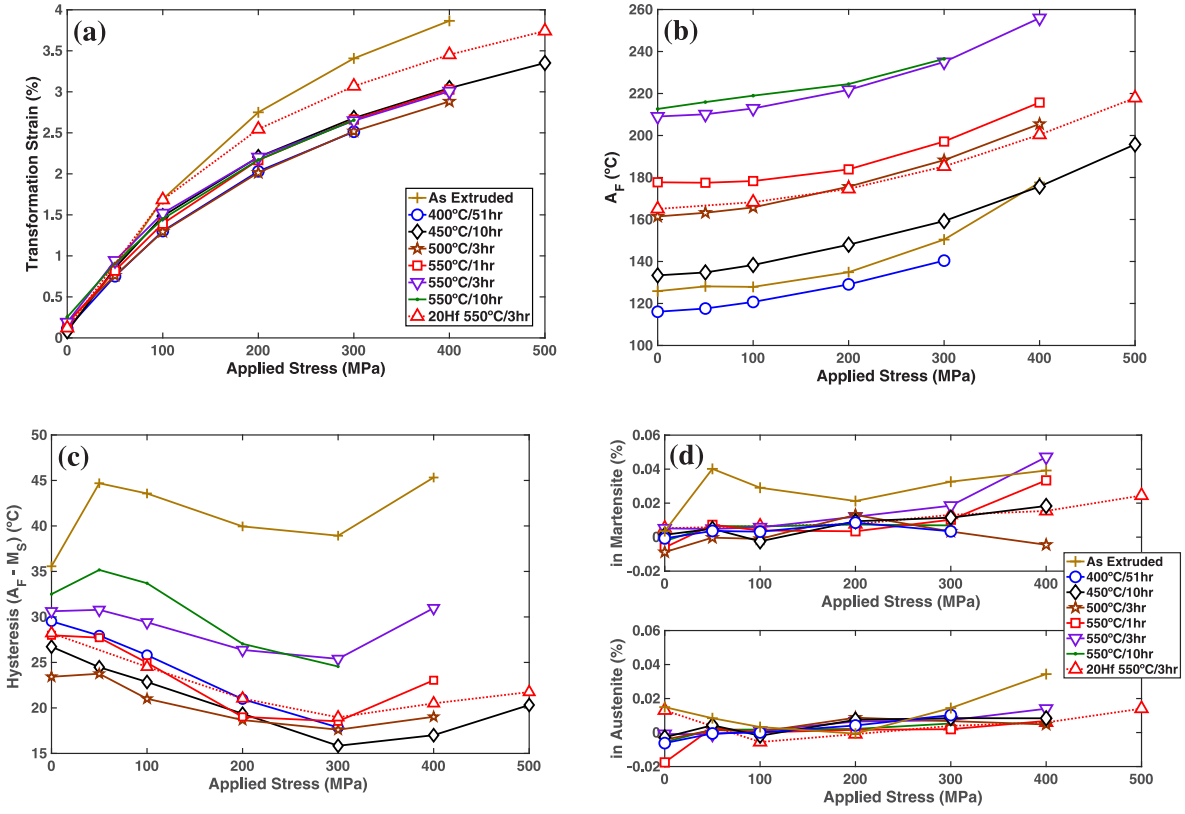

Fig. 3. Summary of constant force shape memory behaviors (a) transformation strain, (b) austenite finish temperature, (c) hysteresis, and (d) residual strain in the martensite and austenite of the as-extruded and aged $Ni_{50.5}Ti_{27.2}Hf_{22.3}$ alloy with comparison to a baseline 550 °C/3h aged $Ni_{50.3}Ti_{29.7}Hf_{20}$ alloy.

transformation temperature and increased precipitate size. Thus, a one hour age at 550 °C resulted in an average increase of 55 °C over the as-extruded condition. When aged for 3 h at 550 °C, the temperatures increased an additional 35 °C. However, after three hours of aging, the kinetics driving precipitation have slowed significantly due to the precipitation of the H-phase depleting the matrix Ni content, such that seven more hours (a total aging time of 10 h) only improve the transformation temperatures by an additional 2 °C (average of 92 °C total over the as-extruded condition).

Fig. 3a depicts the transformation strain observed during thermomechanical cycling. As with the 20Hf alloy reported previously [1], transformation strain for all conditions increases with increasing stress up to failure at 400 or 500 MPa, indicating that the maximum transformation strain capability of the material has not yet been reached (*i.e.* there is no peak in the transformation strain versus stress curve). Compared to the 20Hf alloy aged at 550 °C for three hours, the as-extruded condition exhibited higher transformation strain at all stress levels. However, transformation strain for all the aged conditions was lower than that of the as-extruded condition due partly to a decrease in transformable volume from precipitation. The lowest strains were seen in the 500 °C/3 h and 400 °C/51 h conditions with 2.51% at 300 MPa (both) and 2.88% at 400 MPa (500 C/3 h condition). All other conditions had equivalent strains of 3.0% under 400 MPa stress.

The effect of ageing on the austenite finish temperature (A_F) as a function of applied stress is shown in Fig. 3b. Similar to other studies in NiTiHf and NiTiZr alloys, aging at low temperature (400 °C) produced a decrease in the transformation temperature, most likely due to a decrease in the H-phase interparticle spacing. With higher aging temperatures, the chemical effects dominate, and the A_F increases over that of the as-extruded condition, with the effect of aging more pronounced at higher aging temperatures. Aging also affects the stress sensitivity (the magnitude of transformation temperature rises with increasing stress) through the strengthening effect of the precipitate phase. Thus, the as-extruded condition (without precipitates) exhibits a higher stress sensitivity than the aged conditions which have precipitates which strengthen the microstructure against deformation and plastic effects.

Fig. 3c shows the effect of heat treatment and stress on the hysteresis (A_F-M_S). It can be seen that the hysteresis for the as-extruded condition is significantly higher than for the aged conditions due to the lack of precipitation strengthening. With aging, the hysteresis decreases, due to the strengthening effect of the precipitated H-phase. This effect is most pronounced with low temperature aging (400–500 °C), or low aging times (550 °C/1 h), presumably when the size of the H-phase provides the greatest strengthening effect. At the higher 550 °C aging temperature, longer aging times grow the precipitate, resulting in a hysteresis that increases, but is still lower than that of the as-extruded condition. Additionally, for the lower aging temperatures, it can be seen that the hysteresis decreases with increasing applied stress until 300 MPa, above which, the applied stress begins to cause a widening of the hysteresis.

Residual strain is an important measure of material behavior and was calculated as the strain difference between the heating and cooling curves in the martensite (2nd cool – 2nd heat) and austenite (2nd heat – 1st cool) at a specified stress. For the most part, it is a measure of accumulating plasticity, but can be an indicator of other processes occurring, such as reorientation/detwinning in the martensite and retained martensite in the austenite phase. Using the residual strain measurements from both the martensite and austenite, the cause for the residual strain can be better determined. In the studied alloy, the as-extruded material has the highest residual strain (Fig. 3d), as would be expected, due to the lack of precipitates to strengthen the matrix against plasticity. At stresses up to 200 MPa, the as-extruded condition exhibits high residual strain in the martensite, and low, decreasing residual strain in the austenite. This is indicative of: (1) preferential orientation of thermally induced martensite (therefore higher strain in the martensite which is

Table 2
Average residual strain per cycle (x10^{-3} %) from 100 to 300 MPa.

Condition	Martensite	Austenite	M - A
As-extruded	27.63	5.67	21.96
400 °C/51 h	5.04	4.83	0.21
450 °C/10 h	6.10	4.70	1.41
500 °C/3 h	5.09	5.32	-0.23
550 °C/1 h	5.86	1.22	4.64
550 °C/3 h	12.08	4.91	7.17
550 °C/10 h	6.86	3.07	3.80
20Hf 550 °C/3 h	9.10	-0.87	9.96

recovered when transformed to austenite), and (2) self-training, as the material exhibits lower residual strain with additional cycling under stress. At higher stresses though, an increase in the residual strain is seen in austenite as well as the martensite, indicative of plasticity or residual martensite in the matrix. On the other hand, the aged conditions exhibited low residual strain (near perfect dimensional stability), with levels in the martensite at 300 MPa ranging from 3.3×10^{-3}% for the 500 °C/3 h condition to 18.5×10^{-3} % for the 550 °C/3 h condition. Because these strains are very small and approach the detection limit of the extensometer, the average residual strain over the range from 100 to 300 MPa is reported in Table 2. Based on this, it is shown that the average residual strain in the martensite is highest for the as-extruded condition at 27.6×10^{-3}%, and lowest in the 400 °C/51 h and 500°C/3h conditions. In the austenite, the highest average residual strain is also seen in the as-extruded condition at only 5.7×10^{-3}% and lowest in the 550 °C/1 h condition at 1.2×10^{-3}%. The difference between the residual strain in the martensite and in the austenite can give a third indication as to the mechanism responsible for the level of residual strain. In the as-extruded condition, there is an average of 27.6×10^{-3} % strain in the martensite, but only 5.7×10^{-3} % strain in the austenite. Thus, while this condition exhibits the largest residual strain, 22×10^{-3} % is from extension (or additional re-orientation) in the martensite. This agrees well with the higher transformation strain in the as-extruded condition. In the 400 °C/51 h and 500 °C/3 h conditions, nearly all the residual strain exhibited in the martensite also showed up in the austenite, so in these conditions, this small amount of residual strain was due to plastic type processes or retained martensite.

4. Conclusion

Aging heat treatments of a Ni-rich $Ni_{50.5}Ti_{27.2}Hf_{22.3}$ alloy produced transformation temperatures over 200 °C after aging at 550 °C for 3 h, an improvement of over 90 °C from the corresponding as-extruded material, and nearly 50 °C higher than the previously studied $Ni_{50.3}Ti_{29.7}Hf_{20}$ alloy under the same aging condition. Transformation strains in the as-extruded condition were as high as 3.8%, and decreased to a maximum of 3% to 3.4% in the heat-treated conditions. The dimensional stability of the as-extruded material was improved by a factor of 2 – 5 through aging heat treatment, to the point where the residual strain per cycle was negligible and can be considered “in the noise” of the extensometer. Thus, we have shown the viability of a Ni-rich NiTiHf alloy with 22.3 at.% Hf that can be aged to produce a transformation temperature capability of 200 °C, good transformation strains and near perfect dimensional stability.

Declaration of Competing Interest

None

Acknowledgments

This work was supported by the NASA Transformative Aeronautics Concepts Program (TACP), Transformational Tools & Technologies Project (TTT).

References

[1] G.S. Bigelow, A. Garg, S.A. Padula, D.J. Gaydosh, R.D. Noebe, Load-biased shape-memory and superelastic properties of a precipitation strengthened high-temperature $Ni_{50.3}Ti_{29.7}Hf_{20}$ alloy, Scr. Mater. 64 (2011) 725–728, doi:10.1016/j.scriptamat.2010.12.028.
[2] O. Benafan, R.D. Noebe, S.A. Padula, R. Vaidyanathan, Microstructural Response During Isothermal and Isobaric Loading of a Precipitation-Strengthened Ni-29.7Ti-20Hf High-Temperature Shape Memory Alloy, Metall. Mater. Trans. A 43 (2012) 4539–4552 43A, doi:10.1007/s11661-012-1297-z.
[3] O. Benafan, A. Garg, R.D. Noebe, G.S. Bigelow, S.A. Padula, D.J. Gaydosh, N. Schell, J.H. Mabe, R. Vaidyanathan, Mechanical and functional behavior of a Ni-rich $Ni_{50.3}Ti_{29.7}Hf_{20}$ high temperature shape memory alloy, Intermetallics 50 (2014) 94–107, doi:10.1016/j.intermet.2014.02.006.
[4] S.M. Saghaian, H.E. Karaca, H. Tobe, M. Souri, R. Noebe, Y.I. Chumlyakov, Effects of aging on the shape memory behavior of Ni-rich $Ni_{50.3}Ti_{29.7}Hf_{20}$ single crystals, Acta Mater. 87 (2015) 128–141, doi:10.1016/j.actamat.2014.12.040.
[5] A. Evirgen, I. Karaman, F. Basner, R. Santamarta, J. Pons, R.D. Noebe, Microstructural characterization and shape memory characteristics of the $Ni_{50.3}Ti_{34.7}Hf_{15}$ shape memory alloy, Acta Mater. 83 (2015) 48–60, doi:10.1016/j.actamat.2014.09.027.
[6] B.C. Hornbuckle, T.T. Sasaki, G.S. Bigelow, R.D. Noebe, M.L. Weaver, G.B. Thompson, Structure–property relationships in a precipitation strengthened Ni–29.7Ti–20Hf (at%) shape memory alloy, Mater. Sci. Eng. A 637 (2015) 63–69, doi:10.1016/j.msea.2015.03.123.
[7] K.C. Atli, I. Karaman, R.D. Noebe, G. Bigelow, D. Gaydosh, Work production using the two-way shape memory effect in NiTi and a Ni-rich NiTiHf high-temperature shape memory alloy, Smart Mater. Struct. 24 (2015) 125023, doi:10.1088/0964-1726/24/12/125023.
[8] O. Benafan, R.D. Noebe, T.J. Halsmer, Static rock splitters based on high temperature shape memory alloys for planetary explorations, Acta Astronaut. 118 (2015) 137–157, doi:10.1016/j.actaastro.2015.10.009.
[9] H.E. Karaca, S.M. Saghaian, G. Ded, H. Tobe, B. Basaran, H.J. Maier, R.D. Noebe, Y.I. Chumlyakov, Effects of nanoprecipitation on the shape memory and material properties of an Ni-rich NiTiHf high temperature shape memory alloy, Acta Mater. 61 (2013) 7422–7431, doi:10.1016/j.actamat.2013.08.048.
[10] O. Benafan, G.S. Bigelow, A. Garg, R.D. Noebe, D.J. Gaydosh, R.B. Rogers, Processing and scalability of NiTiHf high-temperature shape memory alloys, Shape Mem. Superelasticity 7 (2021) 109–165, doi:10.1007/s40830-020-00306-x.
[11] D.R. Coughlin, L. Caselena, F. Yang, G.S. Bigelow, A. Garg, R.D. Noebe, M.J. Mills, Microstructure–property relationships in a high-strength 51Ni–29Ti–20Hf shape memory alloy, J. Mater. Sci. 51 (2016) 766–778, doi:10.1007/s10853-015-9400-7.
[12] L. Patriarca, H. Sehitoglu, High-temperature superelasticity of $Ni_{50.6}Ti_{24.4}Hf_{25.0}$ shape memory alloy, Scr. Mater. 101 (2015) 12–15, doi:10.1016/j.scriptamat.2015.01.005.
[13] L. Patriarca, H. Sehitoglu, E.Y. Panchenko, Y.I. Chumlyakov, High-temperature functional behavior of single crystal $Ni_{51.2}Ti_{23.4}Hf_{25.4}$ shape memory alloy, Acta Mater. 106 (2016) 333–343, doi:10.1016/j.actamat.2016.01.015.
[14] L. Patriarca, Y. Wu, H. Sehitoglu, Y.I. Chumlyakov, High temperature shape memory behavior of $Ni_{50.3}Ti_{25}Hf_{24.7}$ single crystals, Scr. Mater. 115 (2016) 133–136, doi:10.1016/j.scriptamat.2016.01.015.
[15] A.N. Bucsek, G.A. Hudish, G.S. Bigelow, R.D. Noebe, A.P. Stebner, Composition, compatibility, and the functional performances of ternary NiTiX high-temperature shape memory alloys, Shape Mem. Superelasticity 2 (2016) 62–79, doi:10.1007/s40830-016-0052-5.
[16] F. Yang, D.R. Coughlin, P.J. Phillips, L. Yang, A. Devaraj, L. Kovarik, R.D. Noebe, M.J. Mills, Structure analysis of a precipitate phase in an Ni-rich high-temperature NiTiHf shape memory alloy, Acta Mater. 61 (2013) 3335–3346, doi:10.1016/j.actamat.2013.02.023.
[17] R. Santamarta, J. Pons, A. Evirgen, R. Arroyave, I. Karaman, H.E. Karaca, R.D. Noebe, TEM study of structural and microstructural characteristics of a precipitate phase in Ni-rich Ni–Ti–Hf and Ni–Ti–Zr shape memory alloys, Acta Mater. 61 (2013) 6191–6206, doi:10.1016/j.actamat.2013.06.057.
[18] ASTM E3097-17Standard Test Method for Mechanical Uniaxial Constant Force Thermal Cycling of Shape Memory Alloys, ASTM International, West Conshohocken, PA, 2017 www.astm.org.
[19] X.L. Meng, Y.D. Fu, W. Cai, J.X. Zhang, Q.F. Li, L.C. Zhao, Martensitic Transformation Behavior and Shape Memory Effect of an Aged Ni-rich Ti-Ni-Hf High Temperature Shape Memory Alloy, Solid State Phenom. 138 (2008) 399–406, doi:10.4028/www.scientific.net/SSP.138.399.
[20] Tejas Umale, Daniel Salas, Bradley Tomes, Raymundo Arroyave, Ibrahim Karaman, The effects of wide range of compositional changes on the martensitic transformation characteristics of NiTiHf shape memory alloys, Scripta Materialia 161 (2019) 78–83, doi:10.1016/j.scriptamat.2018.10.008.
[21] Othmane Benafan, Glen Bigelow, Anita Garg, Ronald Noebe, Darrell Gaydosh, Richard Rogers, Processing and Scalability of NiTiHf High-Temperature Shape Memory Alloys, Shape Memory and Superelasticity 7 (2021) 109–165, doi:10.1007/s40830-020-00306-x.